Jet emission spectroscopy of OH and OD near 1850 Å: First observation of a 2Π→2Π electronic transition of OD

K. P. Huber, F. Holland, and J. A. Coxon

Citation: J. Chem. Phys. **96**, 1005 (1992); doi: 10.1063/1.462187
View online: http://dx.doi.org/10.1063/1.462187
View Table of Contents: http://jcp.aip.org/resource/1/JCPSA6/v96/i2
Published by the American Institute of Physics.

Jet emission spectroscopy of OH and OD near 1850 Å: First observation of a $^2\Pi \rightarrow {}^2\Pi$ electronic transition of OD

K. P. Huber[a] and F. Holland[b]
Herzberg Institute of Astrophysics, National Research Council of Canada, Ottawa, Ontario K1A OR6, Canada

J. A. Coxon
Department of Chemistry, Dalhousie University, Halifax, Nova Scotia B3H 4J3, Canada

(Received 12 September 1991; accepted 7 October 1991)

The complex many-line systems observed at around 1850 Å from discharges containing H_2O or D_2O [A. Michel, Z. Naturforsch. **12a**, 887 (1957); P. Felenbok and J. Czarny, Annu. Astrophys. **27**, 244 (1964)] have been reinvestigated at high resolution in the emission from supersonic jet expansions. Mixtures of He with D_2O produce a conspicuous progression of red shaded bands that overlap the many-line spectra but have not been reported before. The new transitions originate at large internuclear distance in a single $^2\Pi$ vibronic level of OD at 88 294 cm^{-1} above the minimum of the ground-state potential, and they end on high vibrational levels, $v'' = 13,...,18$, of $X\,^2\Pi$. Term values and spectroscopic parameters for the initial and final states have been determined; the upper state, labeled $C'\,^2\Pi$, is inverted with a spin-orbit interaction that is close to the A value of $X\,^2\Pi_i$. Analogous bands of OH have not been detected, and in contrast with the many-line emissions of both isotopes which persist in the presence of Ar as well as of He and in discharges through pure water vapor, the new $C'\,^2\Pi \rightarrow X\,^2\Pi$ bands of OD appear only in mixtures with He. Guided by *ab initio* calculations for the $^2\Pi$ excited states of OH [E. F. van Dishoeck and A. Dalgarno, J. Chem. Phys. **79**, 873 (1983)], the interpretation of the experimental results concludes that all of the observed emission at around 1850 Å originates in a group of more or less strongly mixed $^2\Pi$ levels which reflect the radiative properties and excitation characteristics of two interacting stable diabatic states and which escape predissociation by a repulsive third $^2\Pi$ state.

I. INTRODUCTION

For over sixty years the hydroxyl radical has captivated the interest of experimental and theoretical spectroscopists alike, their curiosity being motivated by a wide range of observations concerning the occurrence of OH in high-temperature gases and in various flames and discharges, by the role the radical plays as a catalyst and intermediary in the increasingly important field of atmospheric chemistry, by its prominence in cometary spectra, and by its presence both in stellar atmospheres and in the interstellar medium. Most of the efforts have been directed towards a detailed understanding of the molecule in its $X\,^2\Pi_i$ ground state, with relatively few investigations focused on the electronically excited molecule. The 1977 compilation by Huber and Herzberg[1a] mentions only four excited states, $A\,^2\Sigma^+$, $B\,^2\Sigma^+$, $D\,^2\Sigma^-$, and $C\,^2\Sigma^+$ in order of increasing energy, and a second member of the Rydberg series beginning with $D\,^2\Sigma^-$ has recently been identified by de Beer *et al.*[1b] in a $(2+1)$ resonantly enhanced multiphoton ionization study of OH and OD. Particularly striking is the absence of electronically excited states having non-Σ symmetries, in sharp contrast to *ab initio* calculations by Easson and Pryce[2] and by van Dishoeck and Dalgarno[3] who find several bound $^2\Pi$ and $^2\Delta$ states at energies comparable to those of the $^2\Sigma$ states.

In the light of these calculations it appears possible that transitions from at least one of several strongly interacting $^2\Pi$ states might contribute to a long known but little understood system of emission lines at around 1850 Å. Michel[4] first observed the emission in the course of a reinvestigation of the $C\,^2\Sigma^+ \rightarrow A\,^2\Sigma^+$ bands near 2500 Å while extending the search for new bands of this system into the Schumann region of the spectrum. Working with a relatively low dispersion corresponding to about 8.3 Å/mm he detected a very complex system of emission lines that appeared between 1900 and 1750 Å under the same experimental conditions as, but with considerably higher intensity than, the known $C \rightarrow A$ bands at longer wavelengths. The spectrum was emitted from a hollow cathode or high-frequency discharge in pure water vapor, and experiments with D_2O and samples containing 10% of ^{18}O led to the conclusion that the most likely carrier of the spectrum was a molecule built from a single hydrogen atom and not more than two oxygen atoms.

Felenbok and Czarny[5,6] confirmed the existence of the new many-line spectrum, noticing that the emission lines accumulate near 1850 Å and reach a long-wavelength limit at about 1894 Å, or 52 800 cm^{-1}, i.e., at an energy similar to the excitation of the $C\,^2\Sigma^+$ state of the hydroxyl radical above the $^3P + {}^2S$ dissociation limit of the $X\,^2\Pi_i$ ground state. Consequently, they interpreted the emission in terms of transitions from $C\,^2\Sigma^+$ to very high vibrational levels in $X\,^2\Pi_i$, a view that is compatible with the more-than-twofold increase of the equilibrium internuclear distance in the up-

[a] Author to whom correspondence should be addressed.
[b] Present address: Forschungszentrum Jülich GmbH, Institut für Atmosphärische Chemie, D-5170 Jülich, Germany.

per state over the ground-state value, and which gains some support from the lifetime measurements of Bergeman, Erman, and Larsson[7] at various wavelengths of the many-line spectrum, the upper-state lifetimes being approximately the same as for the C state observed in $C \rightarrow A$ transitions.

High-resolution spectra of the 1850 Å emission have been available for some time; at a dispersion of ~0.25 Å/mm they have been photographed by Alberti and Douglas[8] on the 10.7 m normal incidence vacuum spectrograph of the National Research Council in Ottawa, and by Czarny and Felenbok[9] using a similar instrument at the National Institute of Standards and Technology in Washington. As in previous investigations, the spectra were produced from hollow cathode or microwave discharges in pure H_2O or D_2O vapor, or in 50% mixtures of $H_2O + D_2O$. They consist of a large number of fairly distinct clusters of lines, each group being made up of around ten to thirty lines which, for the most part, are well resolved. However, the lines do not organize into a number of emerging branches, providing no clues as to how and where the analysis of this system might start. Isotope studies definitely rule out the possibility of more than one hydrogen atom being present in the radiating molecule, and the relatively open appearance of the spectra tends to further restrict the choice of possible candidates to the light diatomic species OH and OD or their cations.

The supersonic expansion experiments reported here were carried out in the hope that they might produce rotationally cold spectra and thus lead to the identification of low-J transitions in the many-line emissions near 1850 Å. These expectations were only partially fulfilled; a comparison with the spectra recorded by Alberti and Douglas[8] under equilibrium conditions reveals substantial changes in the relative intensities of the lines, but for the most part, the supersonic expansion spectra remain just as chaotic as those obtained from standard discharges. The one notable exception is that in the emission from a jet expansion of $He + D_2O$, the formless many-line spectrum unexpectedly gives way to the regular structure of a progression of bands which forms the subject of this communication. The bands arise in a $^2\Pi \rightarrow {}^2\Pi$ transition of OD and correspond to the strongest of such transitions predicted by the calculations of van Dishoeck and Dalgarno.[3] They originate at large internuclear distance from a single $^2\Pi$ vibronic level, labeled C', which lies at only 1635 cm^{-1} below $v = 0$ of $C\,^2\Sigma^+$ and seems to be free of perturbations by neighboring discrete and continuum states of $^2\Pi$ symmetry,[3,10] and they end on six consecutive vibrational levels in the ground-state potential of OD, the highest two of these, $v = 17$ and 18, being just above the $v = 12$ level recently observed in a laser double-resonance study of OH.[11,12]

II. EXPERIMENTS AND OBSERVATIONS

As shown in Fig. 1, the emission is generated in a nozzle discharge of the type used earlier for a study of the CN radical.[13] Pure He or Ar mixed with H_2O or D_2O expands from a reservoir pressure of typically 1.5 atmospheres through a quartz nozzle of ~0.3 mm diam into a Plexiglas chamber mounted directly on top of a high-speed EDWARDS EH500/E2M80 pump combination with a capacity of 140 l/s. The discharge current of ~100 mA is maintained by a voltage close to 1 kV applied to the tungsten anode inside the quartz tube. The light emitted from the jet discharge passes through a foreslit and is collected by a lithium fluoride lens for predispersion by a suprasil or lithium fluoride prism/cylinder combination before entering into the 10.7 m vacuum spectrograph where it is photographed in the sixth order of a 600 lines/mm concave grating at an inverse dispersion of about 0.25 Å/mm.

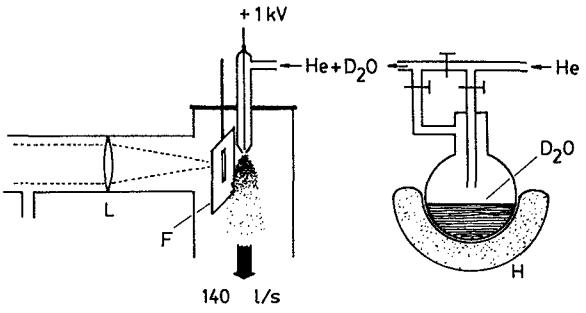

FIG. 1. Schematic diagram of the jet discharge experiments using mixtures of rare gases with H_2O or D_2O. L, lithium fluoride spherical lens; F, foreslit; H, heater.

The rare-gas flow entrains water vapor over a suitably heated sample of liquid H_2O or D_2O. The water content of the gas flow was not measured, but it is readily monitored by observing the reddish tint of the discharge due to emission in the Balmer H_α line. Excess water leads to rapid ice formation at the nozzle exit, interrupting the expansion or, at the very least, blocking the light from the most brilliant part of the corona discharge. Under optimum conditions, and using slit widths of 20 or 30 μ, the high-resolution spectra reported here were photographed in 3–6 h on ILFORD Q2 plates, with Fe lines added in overlapping orders for calibration purposes.

Figure 2 shows photometer traces of first-order spectra obtained under comparable conditions with the four gas mixtures indicated in the left margin of Fig. 2. With Ar as the carrier gas, both H_2O and D_2O produce only weak emission in the many-line systems attributed to OH and OD [Figs. 2(a) and 2(d)]. When Ar is replaced by He, the intensity of the spectrum emitted from the H_2O mixture increases dramatically, so much so that most of the lines between 1800 and 1870 Å become totally saturated [Fig. 2(b)]. By contrast, the spectrum from the D_2O mixture not only gains in intensity, but at the same time radically changes its character [Fig. 2(c)]; what appears in Ar as a structureless accumulation of lines, reveals in He a long lower-state progression of bands which extends with increasing vibrational intervals and diminishing intensities from 1873 Å to shorter wavelengths. Additional bandheads can be seen at 1839, 1802, and 1762 Å, and—not reproduced in Fig. 2—at 1721 and 1679 Å, before the progression submerges into the very much stronger Lyman bands of D_2 which appear simultaneously with the new bands and, like the latter, are absent when the discharge is running in $Ar + D_2O$ rather than $He + D_2O$.

The high-resolution spectrum of one of the red shaded bands is reproduced in Fig. 3; it will be seen to arise in a

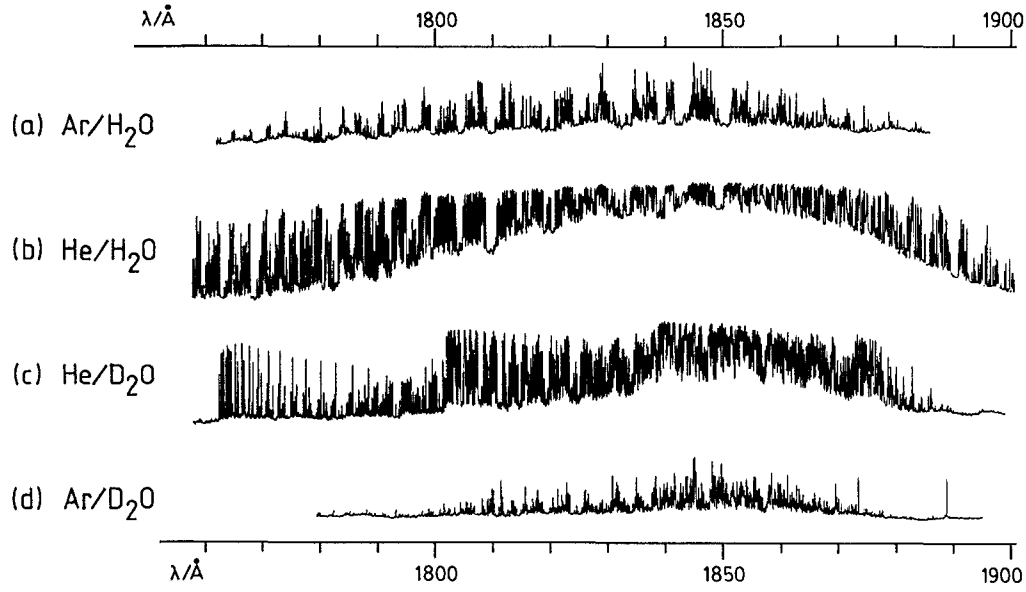

FIG. 2. Jet emission spectra of four rare-gas/water mixtures between 1760 and 1900 Å. These are photometer traces of first-order spectra photographed at a plate dispersion of 0.77 Å/mm.

transition to $v = 16$ of the $X\,^2\Pi_i$ ground state of OD. The rotational structure is well resolved and consists of two overlapping subbands of a $\Delta\Lambda = 0$ transition where both upper and lower states follow case a coupling conditions with nearly identical values for the spin–orbit coupling constant A. The $^2\Pi_{3/2} \rightarrow {}^2\Pi_{3/2}$ subband has three strong branches, one R, one P, and a short Q branch, the lines being single for all but the very highest observed J values where a slight broadening or incipient doubling can be seen. The underlying $^2\Pi_{1/2} \rightarrow {}^2\Pi_{1/2}$ subband is less conspicuous; it comprises an R and a P branch of widely split doublets but gives no indication of Q-branch transitions, in accordance with the very low predicted intensities of the latter. The decomposition of each rovibronic transition into two well-separated Λ-type doubling components accounts, by and large, for the apparent weakness of this subband, although the partial depopulation

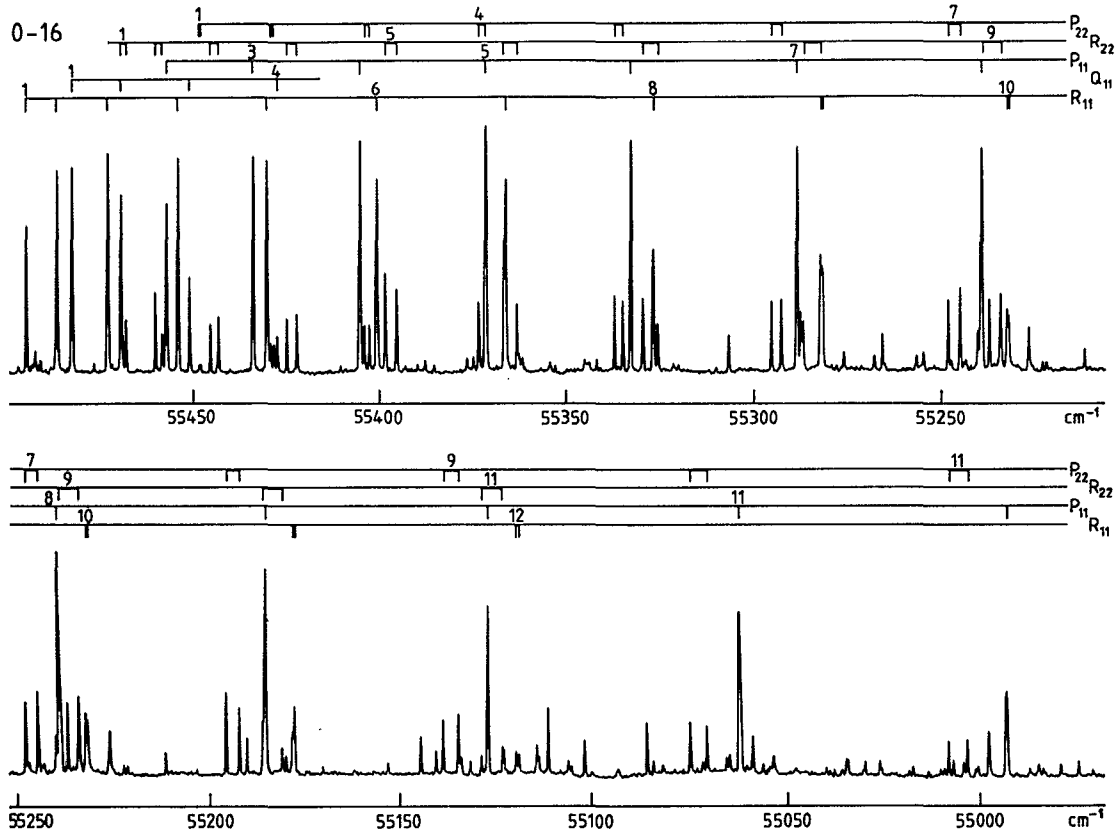

FIG. 3. The 0-16 band in the $C'\,^2\Pi_i \rightarrow X\,^2\Pi_i$ transition of ^{16}OD, photographed on the 10.7 m vacuum spectrograph in the sixth order of a 600 lines/mm concave grating; the plate dispersion is 0.25 Å/mm.

TABLE I. Observed wave numbers (in cm^{-1}) and residuals for the $C'^2\Pi_i \rightarrow X^2\Pi_i$ transitions of ^{16}OD. Residuals (obs-calc) are given in parentheses in units of the last quoted figure. Calculated transition wave numbers are given without residuals. Transition wave numbers indicated by an asterisk (*) were not included in the fit.

$J-\frac{1}{2}$	R_{11ee}	R_{11ff}	Q_{11ef}	Q_{11fe}	P_{11ee}	P_{11ff}	R_{22ee}	R_{22ff}	P_{22ee}	P_{22ff}
					0-13					
0							59 535.48	59 536.36		
1	59 560.09(− 16)*	59 560.09(− 17)*	59 547.96(− 4)	59 547.96(− 5)			528.39	529.68	59 508.38	59 508.75
2	547.32(14)	547.32(13)	529.94(− 10)	529.94(− 12)	59 517.76(− 5)	59 517.76(− 4)	513.33	515.03	483.11	483.90
3	526.94(4)	526.94(2)	504.81(− 7)	504.81(− 13)	487.78(0)	487.78(2)	490.39(6)	492.42(− 3)	449.93	451.15
4	499.43(2)	499.43(− 1)			450.59(1)	450.59(5)	459.64(18)*	461.95(− 3)	408.85(− 6)	410.53(− 4)
5	464.71(1)	464.71(− 3)			406.24(5)	406.24(10)	420.75(− 2)	423.68(− 3)	360.14(0)	362.26(2)
6	422.85(8)	422.85(3)			354.63(0)	354.63(6)	374.48(13)	377.73(3)	303.71(0)	306.28(4)
7	373.68(5)	373.68(− 2)			295.87(− 5)	295.87(3)	320.28	324.05	239.71(1)	242.47(− 20)*
8	317.33(4)	317.33(− 5)			230.06(− 2)	230.06(8)	258.62(− 4)	262.74(− 11)	168.25(3)	171.81(17)*
9	253.81(2)	253.81(− 10)			157.09(− 7)	157.09(5)	189.50(− 8)	194.27(8)	089.43(4)	093.26(0)
10	183.26(9)	183.26(− 6)			077.12(− 7)	077.12(5)	113.25(10)	118.13(− 5)	003.27(− 4)	007.65(2)
11	105.35(− 13)*	105.35(− 31)*			58 990.13(− 11)	58 990.13(2)			58 910.11(0)	58 914.84(− 3)
12	020.79(2)*	020.79(− 20)*			896.29(− 9)	896.29(4)				
13	58 929.39(26)*	58 929.39(− 1)*			795.62(− 7)	795.62(4)				
14					688.26(− 2)	688.26(8)				
15					574.20(− 3)	574.20(5)				
16					453.91(24)*	453.91(29)*				
					0-14					
0							58 070.81	58 071.69		
1	58 095.27(− 3)	58 095.27(− 4)	58 083.01(− 4)	58 083.01(− 5)			064.84(9)	066.05	58 044.74	58 045.12
2	083.67(− 3)	083.67(− 5)	066.51(− 5)	066.51(− 8)	58 054.35(2)	58 054.35(3)	051.33(− 7)	053.07(− 4)	021.17	021.98
3	065.55(6)	065.55(3)	043.60(13)	043.60(7)	026.37(− 1)	026.37(1)	030.81(2)	032.91(− 1)	57 990.35(− 4)	57 991.80(18)*
4	040.71(3)	040.71(0)			57 991.80(− 4)	57 991.80(− 1)	003.01(3)	005.55(3)	952.40(− 4)	954.14(3)
5	009.29(4)	009.29(− 1)			950.73(− 1)	950.73(3)	57 968.02(− 2)	57 971.23(24)*	907.39(− 3)	909.54(2)
6	57 971.23(1)	57 971.23(− 6)			903.06(− 3)	903.06(3)	926.06(2)	929.41(0)	855.41(1)	857.95(1)
7	926.65(3)	926.65(− 6)			848.94(3)	848.94(9)	877.08(1)	880.85	796.45(− 4)	799.49(2)
8	875.52(7)	875.52(− 5)			788.21(− 3)	788.21(4)	820.74(− 47)*	825.39(− 2)	730.78(0)	734.24(3)
9	817.81(4)	817.81(− 11)			721.11(− 2)	721.11(6)	758.53(− 5)	763.25(5)	658.38(− 2)	662.28(1)
10	753.67(5)	753.67(− 13)			647.61(− 2)	647.61(6)	689.34(6)	694.33(2)	579.43(− 2)	583.77(1)
11	683.20(14)	683.20(− 9)			567.78(− 4)	567.78(4)			494.06(0)	498.83(2)
12	606.23(7)*	606.23(− 21)*			481.72(− 4)	481.72(2)			402.28(− 7)	407.42(− 13)
13					389.50(− 7)	389.50(− 2)			304.53(6)	310.08(− 3)
14					291.33(0)	291.33(3)			200.61(6)	206.64(1)
15					187.17(1)	187.17(0)				
16					077.65(46)*	077.65(41)*				
					0-15					
0							56 713.69	56 714.58		
1	56 737.63(− 1)	56 737.63(− 1)	56 725.34(− 5)	56 725.34(− 6)			708.71	710.03	56 688.70	56 689.10
2	727.61(− 1)	727.61(− 2)	710.42(− 6)	710.42(− 8)	56 698.19(− 6)	56 698.19(− 5)	697.21(3)	698.64(− 28)*	667.02(7)	667.91(12)
3	711.64(1)	711.64(− 1)	689.67(6)	689.67(1)	672.48(− 3)	672.48(− 1)	679.05(− 6)	681.28(0)	638.70(0)	640.09(10)
4	689.67(0)	689.67(− 4)	662.79(1)	662.79(− 9)	640.82(− 2)	640.82(1)	654.55(− 1)	657.16(0)	603.94(− 8)	605.70(− 5)
5	661.83(7)	661.83(1)			603.29(4)	603.29(8)	623.61(0)	626.65(2)	563.01(2)	565.18(2)
6	627.99(7)	627.99(0)			559.81(3)	559.81(8)	586.36(4)	589.74(− 3)	515.69(1)	518.27(− 3)
7	588.24(7)	588.24(− 2)			510.48(2)	510.48(8)	542.66(− 12)	546.63(− 2)	462.15(− 5)	465.26(− 2)
8	542.66(12)	542.66(0)			455.34(0)	455.34(8)	493.07(− 2)	497.50(11)	402.69(4)	406.20(2)
9	491.17(7)	491.17(− 8)			394.43(− 3)	394.43(5)	437.26(− 8)	442.06(− 1)	337.14(− 2)	341.11(− 3)
10	433.96(8)	433.96(− 11)			327.85(− 5)	327.85(3)	375.69(2)	380.70(− 12)	265.70(− 13)	270.23(− 4)

TABLE I. (*Continued.*)

$J-\frac{1}{2}$	R_{11ee}	R_{11ff}	Q_{11ef}	Q_{11fe}	P_{11ee}	P_{11ff}	R_{22ee}	R_{22ff}	P_{22ee}	P_{22ff}
11	56 371.10(13)	56 371.10(− 10)			56 255.66(− 7)	56 255.66(0)	56 308.26(9)	56 313.81(6)	56 188.86(6)	56 193.62(− 8)
12	302.40(− 5)*	302.40(− 33)*			177.97(− 9)	177.97(− 2)			106.31(10)	111.29(− 27)*
13	228.31(− 10)*	228.31(− 44)*			094.92(− 6)	094.92(0)			018.18(− 1)	024.07(7)
14					006.60(0)	006.60(3)				
					0-16					
0							55 471.95	55 472.86		
1	55 494.94(− 2)	55 494.94(− 3)	55 482.68(− 3)	55 482.68(− 4)			468.14(1)	469.48(− 2)	55 448.12(0)	55 448.64(7)
2	486.64(0)	486.64(− 2)	469.48(− 3)	469.48(− 5)	55 457.27(0)	55 457.27(0)	458.52(− 1)	460.34(0)	428.28(− 3)	429.19(− 2)
3	473.05(1)	473.05(− 3)	451.04(0)	451.04(− 4)	433.91(− 2)	433.91(− 1)	443.18(0)	445.42(− 1)	402.76(− 2)	404.11(− 3)
4	454.24(6)	454.24(0)	427.39(8)	427.39(0)	405.36(1)	405.36(2)	422.17(3)	424.83(1)	371.58(− 1)	373.38(− 3)
5	430.14(7)	430.14(− 3)			371.58(2)	371.58(2)	395.52(6)	398.53(− 5)	334.87(3)	337.12(1)
6	400.81(7)	400.81(− 7)			332.64(4)	332.64(2)	363.25(2)	366.79(1)	292.63(4)	295.33(2)
7	366.34(11)	366.34(− 8)			288.57(5)	288.57(1)	325.54(− 1)	329.47(− 4)	244.99(2)	248.14(1)
8	326.71(13)	326.71(− 13)			239.43(6)	239.43(− 1)	282.28(− 22)*	286.90(2)	192.10(3)	195.65(− 3)
9	281.75(− 12)	282.28(9)			185.28(5)	185.28(− 5)	234.24(3)	239.04(5)	134.00(− 2)	138.07(1)
10	232.11(− 4)	232.56(− 1)			126.22(5)	126.22(− 10)	180.74(− 5)	185.93(− 4)	070.92(− 3)	075.39(− 3)
11	177.51(− 2)	178.04(0)			062.38(9)	062.38(− 11)	122.25(− 12)	127.98(3)	002.98(− 2)	007.88(− 1)
12	118.06(− 3)	118.78(7)			54 993.77(8)*	54 993.77(− 20)*			54 930.30(− 2)	54 935.63(0)
13					920.46(− 4)	920.86(0)			853.15(10)	858.81(4)
14					842.75(− 10)	843.41(11)				
					0-17					
0							54 353.94	54 354.87		
1	54 375.49(1)	54 375.49(0)	54 363.20(− 3)	54 363.20(− 4)			351.47(7)	352.77(− 2)	54 331.53(14)	54 332.31(45)*
2	369.08(4)	369.08(2)	351.90(− 1)	351.90(− 3)	54 339.64(− 3)	54 339.64(− 3)	343.89(− 4)	345.76(− 1)	313.69(− 1)	314.44(− 20)*
3	358.12(4)	358.12(0)	336.08(0)	336.08(− 4)	318.96(0)	318.96(0)	331.53(− 3)	333.85(0)	291.12(− 3)	292.42(− 14)
4	342.67(5)	342.67(− 2)	315.79(3)	315.79(− 5)	293.80(1)	293.80(1)	314.44(9)	317.05(− 4)	264.20(39)*	265.66(− 1)
5	322.77(7)	322.77(− 3)			264.20(1)	264.20(0)	292.42(5)	295.54(− 1)	231.74(− 1)	234.11(4)
6	298.41(6)	298.41(− 9)			230.25(4)	230.25(1)	265.66(− 5)	269.33(2)	195.00(− 7)	197.87(2)
7	269.69(7)	269.69(− 14)			191.99(8)	191.99(2)	234.38(− 7)	238.47(− 1)	153.84(− 3)	157.11(1)
8	236.70(12)*	236.70(− 16)*			149.44(7)	149.44(− 2)	198.72(1)	203.20(4)	108.39(11)	111.99(4)
9	199.24(− 7)	199.62(− 4)			102.76(9)	102.76(− 4)	158.42(− 18)*	163.38(− 8)	058.39(− 3)	062.52(− 1)
10	157.82(− 7)	158.42(8)			051.95(5)	051.95(− 14)	114.27(0)	119.60(7)	004.38(− 5)	008.98(0)
11	112.32(− 10)	113.12(14)			53 997.17(− 1)	53 997.47(3)			53 946.43(− 5)	53 951.52(7)
12					938.51(− 13)	939.07(10)				
13					876.43(2)	877.11(27)*				
					0-18					
1	53 390.08(0)	53 390.08(− 1)	53 377.78(− 6)	53 377.78(− 6)						
2	385.74(− 1)	385.74(− 3)	368.66(4)	368.66(3)	53 356.43(5)	53 356.43(5)				
3	377.78(4)	377.78(− 1)	355.57(− 17)*	355.57(− 20)*	338.62(0)	338.62(− 1)				
4	366.19(10)	366.19(2)			317.25(− 1)	317.25(− 2)				
5	350.88(3)	350.88(− 9)			292.32(− 2)	292.32(− 5)				
6	332.13(8)	332.13(− 10)			263.95(3)	263.95(− 2)				
7	309.94(16)*	309.94(− 8)*			232.12(5)	232.12(− 4)				
8	284.54(44)*	284.54(11)*			196.97(7)	196.97(− 6)				
9					158.65(16)*	158.65(− 3)*				

of the $\Omega = \frac{1}{2}$ levels by spin–orbit cooling of the radiating $^2\Pi_i$ state might be a contributing factor. Very rough estimates of the rotational temperatures of the $^2\Pi \rightarrow {}^2\Pi$ emission bands range from ~150 to 250 K, high by comparison with the temperatures achieved in jet emission spectra of stable species, but not out of line with observations on CN and ND_4 free radicals which were produced and excited in free jet expansions of Ar + HCN (Ref. 13) and Ar + ND_3 (Ref. 14).

III. ANALYSES AND RESULTS

The rotational analyses of the six red shaded bands of OD are straightforward. Observations of the first lines in many of the branches facilitate the rotational numbering of the lines which is readily checked and extended to other bands with the help of combination differences for the common upper $^2\Pi$ level. Table I collects the line measurements and the rotational assignments. The spectra are by no means fully assigned. Particularly towards longer wavelengths there remains a large number of unidentified lines, some of which form short segments of branches that appear in the spectra of Ar + D_2O as well as of He + D_2O.

The vibrational numbering used in Table I for the lower state levels, $v'' = 13,...,18$, is unambiguous and will become evident from a comparison of the molecular parameters derived below with those obtained for overlapping vibronic levels of OH. By contrast, the vibrational numbering for the initial state, $v' = 0$, is uncertain; arguments in its favor will be discussed in Sec. IV.

Our choice of e and f labels[15] for the two components of a Λ-type doublet derives from the observation that the splittings in the $\Omega = \frac{1}{2}$ subbands arise almost entirely in the upper state where strong rotational interactions with the nearby $C\,^2\Sigma^+$ state are indicated by the conspicuously large spin splitting constants of the latter.[16] It turns out that this choice of parity labels leads to lower-state parameters which are in line with the Λ-type doubling in the already known ground-state levels of the hydroxyl radical.[17–19]

The data reduction makes use of the effective Hamiltonian of Brown, Colbourn, Watson, and Wayne[20] in the matrix representation of Amiot, Maillard, and Chauville.[21] The diagonalization of upper- and lower-state matrices is followed by a simultaneous least-squares fit of the calculated to the observed transition wave numbers of all six bands. The final adjusted parameters are shown in Table II for the lower-state levels, $v'' = 13,...,18$ of $X\,^2\Pi_i$, and in the first column of Table III for the upper-state level, probably $v' = 0$ of the new $C'^2\Pi_i$ state.

The mass-reduced plots in Figs. 4–8 review the parameters of Table II in the context of previous results for OH, OD, and OT;[17–19] the new data are emphasized in Figs. 4–8 with the help of solid circles. The vibrational intervals and rotational constants in Fig. 4 are seen to link up perfectly with the parameters for the well established lower regions of the ground-state potential, leaving no doubt about the carrier of the spectrum and confirming the vibrational numbering already adopted in Table I; changing v'' by ± 1 introduces serious discontinuities into the plots of Fig. 4 which vastly exceed the experimental uncertainties.

The lack of information on satellite branches makes it difficult to separate the upper state from the lower-state spin splittings. Initially, and in order to break the correlation, the spin–orbit coupling constant A'' for one lower-state level, $v'' = 13$, was held fixed at the value estimated by interpolation between the nearest overlapping OH levels, $v'' = 9$ and 10 (see Fig. 5). Similarly, the identification of only one subband connecting with $v'' = 18$ makes it necessary to guess the coupling strength of this level by extrapolation from observations at lower vibronic energies. For the final calculations of Table II, the fixed parameters were taken from a comprehensive treatment of ground-state data for all three isotopes OH, OD, and OT;[22] a brief explanation of this global fitting approach will be given later.

Figures 5–7 illustrate the rapid changes that take place in the spin–orbit and Λ-type doubling parameters as the molecule approaches the $^3P + {}^2S$ dissociation limit of the ground state. The spin–orbit interaction A rises sharply in order to meet the coupling conditions in the oxygen ^3P term manifold,[23] and the Λ-type doubling is less and less determined by interactions with the $A\,^2\Sigma^+$ state, but is more and more influenced by the unstable $^2\Sigma^-$ state arising from the same dissociation limit. This competition produces the sign change of p near $v = 12$ of OH and $v = 17$ of OD, in perfect agreement with theory[24] which predicts a similar sign change for q at energies that are just beyond the range of the present observations. The theoretical calculations are shown in Figs. 5–7 by solid lines.

TABLE II. Spectroscopic parameters (in cm^{-1}) of different vibrational levels in the $X\,^2\Pi_i$ state of ^{16}OD determined in a least-squares fit to the observed transition wave numbers listed in Table I. Standard deviation of the fit: $\sigma_{fit} = 0.057\ cm^{-1}$ (see Table III). Standard errors (1σ) are given in parentheses in units of the last quoted figure. Parameters without error quotation were obtained in a global fit of data relating to the three isotopes OH, OD, and OT (see text) and were held fixed in the present fit.

	$v = 13$	$v = 14$	$v = 15$	$v = 16$	$v = 17$	$v = 18$
T	0.0	1465.568(20)	2823.773(20)	4066.852(19)	5186.557(21)	6171.713(27)
A	− 139.9549	− 139.427(32)	− 138.624(32)	− 137.383(31)	− 135.585(32)	− 132.5904
$A_D/10^{-2}$	0.176(43)	0.276(35)	0.433(38)	0.498(38)	0.726(41)	
B	6.301 94(52)	5.983 93(47)	5.644 55(51)	5.279 97(49)	4.879 77(59)	4.4394(17)
$D/10^{-3}$	0.5334(23)	0.5596(19)	0.5930(23)	0.6421(22)	0.7040(33)	0.777(23)
p	0.057 23	0.0532(35)	0.0421(36)	0.0138(36)	0.002 95	− 0.021 95
$q/10^{-2}$	− 0.578	− 0.552(28)	− 0.591(31)	− 0.342(32)	− 0.318(32)	− 0.241
$\gamma/10^{-1}$	− 0.363	− 0.340	− 0.317	− 0.293	− 0.268	− 0.243

TABLE III. Spectroscopic parameters (in cm^{-1}) of the $C'^2\Pi_i$ $(v=0)$ state of ^{16}OD determined in the least-squares fits to the observed transition wave numbers and to the term values listed in Tables I and IV, respectively. Standard errors (1σ) are given in parentheses in units of the last quoted figure. Parameters without error quotation were held fixed in the fit.

	Fit to lines	Fit to term values
T	59 547.315(16)[a]	88 294.2827(82)[b]
A	−117.035(25)	−117.105(13)
$A_D/10^{-2}$	−0.723(35)	−0.780(12)
B	2.506 56(44)	2.507 17(21)
$D/10^{-3}$	0.1979(21)	0.1895(11)
p	0.4741(31)	0.4786(28)
$p_D/10^{-4}$	0.81(23)	1.16(21)
$q/10^{-2}$	−0.646(32)	−0.787(23)
σ_{fit}	0.057	0.024

[a] Term value relative to $X^2\Pi_i$ $(v=13)$ of ^{16}OD.
[b] Term value relative to the minimum of the $X^2\Pi_i$ potential curve.

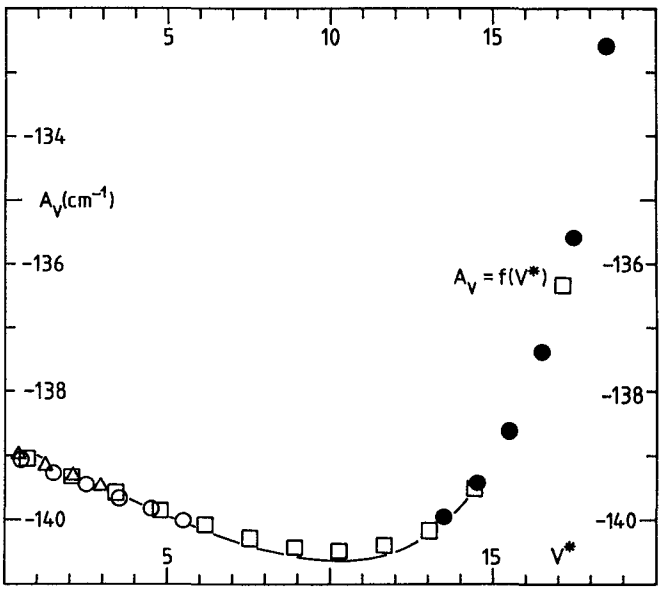

FIG. 5. The spin–orbit interaction parameters A_v in the ground states of OH (open squares), OD (open and solid circles), and OT (open triangles) plotted on a mass-reduced scale. $V^* = \rho(v+1/2)$, where ρ^2 is the ratio of the reduced masses μ relative to μ_{OD}. The solid line refers to the theoretical results for OH from Ref. 23.

Of the centrifugal distortion constants for the lower-state levels, only D_v and A_{Dv} have been determined. The latter, usually strongly correlated with γ, were obtained by restricting the spin–rotation interaction to estimates which derive from the aforementioned global fit of data for three isotopes. There are no theoretical calculations which refer to the vibrational levels observed here, but the results for $v=0$–6 of OH by Langhoff *et al.*[23] are seen to rise steadily from a local minimum at $v=2$, $A_{D2} = -7.4\times10^{-4}\,cm^{-1}$, to $-4.1\times10^{-4}\,cm^{-1}$ at $v=6$, and this trend seems to continue at an accelerated rate between $v=13$ and 17 of OD. The two data sets are compared on the mass-reduced scale of Fig. 8, together with three values determined by Coxon[25] for $v=0$, 1, and 2 of OD.

The exact energies of the $v=13,\ldots,18$ ground-state levels and, consequently, of the $C'^2\Pi_i$ upper state cannot be derived from the OD data alone since neither the initial nor the final vibronic states considered here are spectroscopically connected to the six lowest levels, $v=0\ldots5$.[21] Instead, they have been estimated by means of a comprehensive fitting approach that takes into account Λ doubling and pure rotation transitions in OH, rotation-vibration bands of OH and OD, $A\rightarrow X$ transitions of OH, OD, and OT, the recently identified $B\leftarrow X$ 0-12 band,[12] and the six $C'\rightarrow X$ bands reported here. Details of the fit will be given elsewhere,[22] but it seems in order to add a brief explanation of the fundamentals of the approach.

The $X^2\Pi_i$ ground-state Hamiltonian is set up in terms of the Born–Oppenheimer potential $V(r)$, the spin–orbit operator $A(r)$, the two operators $p(r)$ and $q(r)$ which describe Λ-type doubling, an effective spin–rotation operator $\gamma(r)$, and the functions $g(r)$, $V_H(r)$, and $V_O(r)$, the first accounting for additional J-dependent Born–Oppenheimer break-

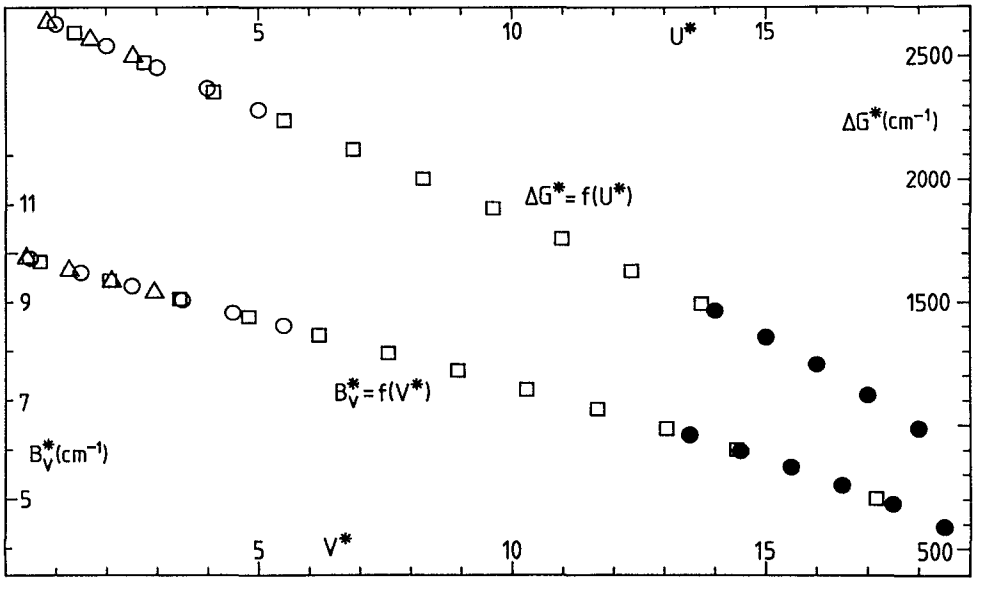

FIG. 4. The ground-state vibrational intervals $\Delta G_{v+1/2}$ and rotational constants B_v of OH (open squares), OD (open and solid circles), and OT (open triangles) plotted on a mass-reduced scale. $\Delta G^* = \Delta G_{v+1/2}/\rho$, $U^* = \rho(v+1)$, $B_v^* = B_v/\rho^2$, and $V^* = \rho(v+1/2)$, where ρ^2 is the ratio of the reduced masses μ relative to μ_{OD}.

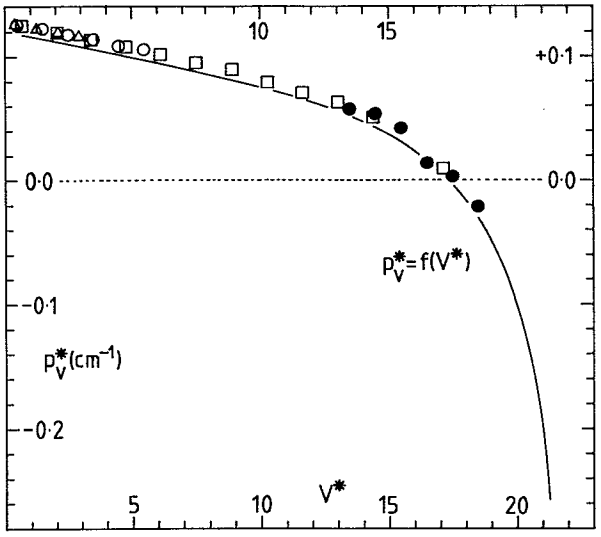

FIG. 6. The Λ-type doubling parameters p_v in the ground states of OH (open squares), OD (open and solid circles), and OT (open triangles) plotted on a mass-reduced scale; $p_v^* = p_v/\rho^2$, $V^* = \rho(v+\frac{1}{2})$, with ρ^2 being the ratio of the reduced masses μ relative to μ_{OD}. The solid line represents theoretical results for OH from Ref. 24.

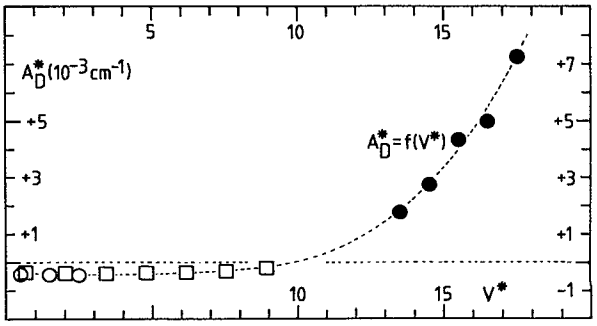

FIG. 8. The centrifugal distortion constants A_{D_v} in the ground states of OH (open squares) and OD (open and solid circles) plotted on a mass-reduced scale; $A_D^* = A_{D_v}/\rho^2$, $V^* = \rho(v+\frac{1}{2})$, and ρ^2 is the ratio of the reduced masses μ relative to μ_{OD}.

down effects, and the latter two, together with $V(r)$, providing effective potentials for each J value of a particular isotope with reduced mass μ. All functions are modeled analytically with sets of adjustable parameters. For each isotope and for each J value, the solution of the radial Schrödinger equation yields four eigenvalues corresponding to two Λ-doubled spin components and, hence, leads to sets of calculated line positions. Adjustments to the parameters are made by standard least-squares procedures. Rather than model the excited $^2\Sigma$ and $^2\Pi$ states, the program finds term values for these states, following the methodology described recently by Watson.[26]

A set of term values for the $C'^2\Pi_i$ upper-state level is shown in Table IV. They refer to the minimum of the ground-state Born–Oppenheimer potential, but are readily converted to energies measured from the lowest existing e and f levels in $X^2\Pi_i(v=0)$ by subtracting $F_{1e}(\frac{3}{2}) = 1309.432$, $F_{1f}(\frac{3}{2}) = 1309.443$, $F_{2e}(\frac{1}{2}) = 1440.425$, or $F_{2f}(\frac{1}{2}) = 1440.529\ cm^{-1}$. Where e and f levels are listed separately, they have been derived exclusively from resolved Λ-type doublets; in particular, the $\Omega = \frac{3}{2}$ e and f levels for $J = 10.5,...,13.5$ are based on measurements in the 0-16 and 0-17 bands alone, with no input from blended lines in other bands of the progression. For other levels the program finds the means of the F_{1e} and F_{1f} terms on the assumption that the blends are composed of lines of equal intensities.

The term values of Table IV reduce to the molecular parameters shown in the second column of Table III, opposite the results obtained in the least-squares fit to the transition wave numbers of Table I. The two sets of constants are in satisfactory agreement, discrepancies generally remaining well within the combined 3σ error limits. However, the absolute reliability of the $C'^2\Pi$ state energy above the minimum of the ground-state potential is limited, as already mentioned, for lack of a direct connection between the lowest ground-state levels $v = 0,...,5$ of OD and the $v = 13,...,18$ levels seen in emission from C'; the true uncertainty exceeds the statistical error quoted in Table III by about 2 orders of magnitude. Finally, combining the relevant energies from Tables II and III with the accepted value for the ground-state dissociation energy, $D_e = 37270\ cm^{-1}$,[1,a] locates the highest observed vibrational level in $X^2\Pi$, $v = 18$ of OD, at about 2281 cm^{-1} below the $^3P + {}^2S$ dissociation limit.

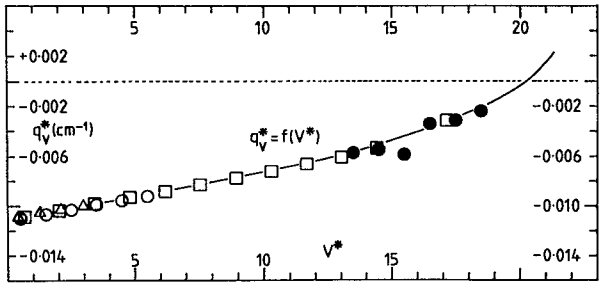

FIG. 7. The Λ-type doubling parameters q_v in the ground states of OH (open squares), OD (open and solid circles), and OT (open triangles) plotted on a mass-reduced scale; $q_v^* = q_v/\rho^4$ and $V^* = \rho(v+\frac{1}{2})$, where ρ^2 is the ratio of the reduced masses μ relative to μ_{OD}. The solid line represents the theoretical results for OH from Ref. 24.

IV. DISCUSSION

The analysis of six bands of OD at wavelengths ranging from 1873 to 1679 Å confirms a suggestion by van Dishoeck *et al.*[3,10] that transitions from an excited $^2\Pi$ state to high vibrational levels in the ground state of OH or OD might contribute to the many-line spectra emitted from discharges containing H_2O or D_2O. The bands appear prominently at the shortest wavelengths of the spectrum generated from a jet discharge in $He + D_2O$ [Fig. 2(c)], but they account for only a fraction of the total emission at longer wavelengths, between 1800 and 1900 Å, where the main contribution comes from a multitude of unassigned lines which can still be seen, weaker but unobstructed, when He is replaced by Ar as the carrier gas of the jet expansion [Fig. 2(d)]. The absence

TABLE IV. Term values (in cm^{-1}) of the $C'^2\Pi_i$ ($v = 0$) state of ^{16}OD. Residuals (obs-calc) are given in parentheses in units of the last quoted figure. Term values indicated by an asterisk (*) were not included in the fit.

	$C'^2\Pi_{3/2}$		$C'^2\Pi_{1/2}$	
	e levels	*f* levels	*e* levels	*f* levels
$J-\frac{1}{2}$	average of *e*, *f*			
0			88 357.69(6)	88 358.24(15)*
1	88 243.08(0)		365.05(−2)	366.04(4)
2	255.31(−2)		377.63(−1)	379.03(0)
3	272.45(−2)		395.27(−5)	397.11(−3)
4	294.50(2)		418.07(1)	420.32(−1)
5	321.37(2)		445.90(1)	448.57(−1)
6	353.08(2)		478.73(0)	481.83(−2)
7	389.58(0)		516.61(4)	520.10(0)
8	430.89(0)		559.37(−1)	563.29(0)
9	476.93(−1)		607.06(−4)	611.40(2)
10	88 527.40(−1)	88 528.01(0)	659.69(2)	664.34(1)
11	582.76(−2)	583.55(1)	717.05(−2)	721.95(−12)*
12	642.79(4)	643.69(−2)	779.24(2)	784.55(1)
13	707.28(−2)	708.46(0)	846.05(0)	851.67(−1)
14	88 776.96(−11)*			

of the red shaded bands from the latter spectrum is readily understood if collisions with rare-gas metastables are the principal excitation mechanism; the $C'^2\Pi$ initial state at approximately 15.9 eV above the ground state of D_2O is well within range of metastable $He(^3S_1)$ with an energy of 19.82 eV, but out of reach for metastable $Ar(^3P_2)$ and $Ar(^3P_0)$ with available energies of only 11.55 and 11.72 eV, respectively. For the very same reason, however, it seems difficult to rationalize the absence of a similar progression of OH bands from the emission of a jet discharge in $He + H_2O$ [Figure 2(b)]; except for a significant drop in intensity, this spectrum does not change substantially when He is replaced by Ar [Figure 2(a)].

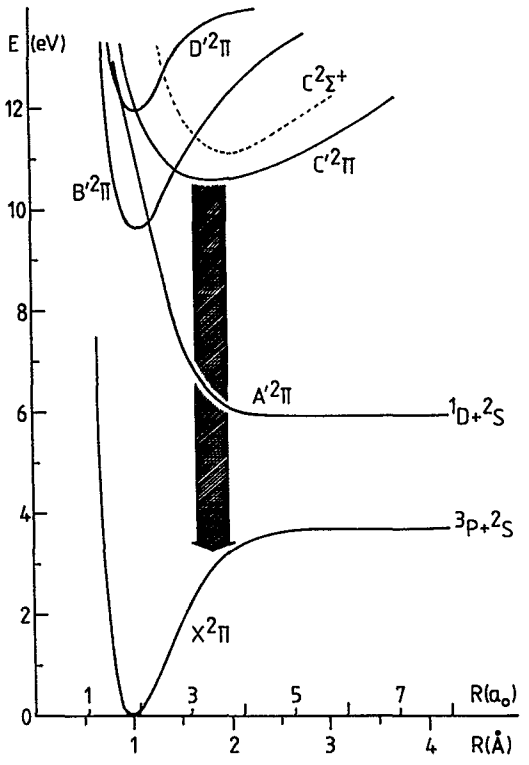

FIG. 9. Approximate diabatic potential curves for the $^2\Pi$ states of the hydroxyl radical, adapted from the *ab initio* calculated adiabatic curves in Fig. 4 of Ref. 3. Also included is the theoretical potential curve for $C^2\Sigma^+$ from Fig. 2 of the same source. The arrow represents the lower-state progression of OD bands observed and analyzed in this work.

The most likely interpretation of the observations—admittedly tentative and incomplete at this stage of the analysis—views the spectra of OH and OD as transitions from a group of upper-state levels that are subject to strong interference from neighboring states. The lack of any regularity in the spectrum of OH suggests that all of the initial levels are severely perturbed; by contrast, one vibrational level of OD escapes such interactions and emits a single lower-state progression of well-behaved bands. The existence of widespread configuration interactions among the $^2\Pi$ excited states of the hydroxyl radical has been demonstrated by the *ab initio* calculations of van Dishoeck *et al.*;[3,10] Fig. 9 shows the participating Π states in a diabatic representation. These are approximate potential curves which have been adapted from a similar figure of adiabatic curves in Ref. 3. They violate the noncrossing rule for states of the same symmetry, but at the same time reveal more clearly the roots of the complications that have, so far, prevented a full analysis of the VUV emission spectra.

There is little doubt that the new progression of OD bands originates in a low vibrational level, probably $v = 0$, of $C'^2\Pi_i$. The initial internuclear distance is 1.9388 Å, slightly longer than the estimated equilibrium distance of 1.85 Å for the C' state, and the intensity distribution along the progression displays the single maximum that normally characterizes the emission from a $v = 0$ level. In the adiabatic representation used by van Dishoeck and Dalgarno (cf. Fig. 4 of Ref. 3), the transition originates in the flat outer part of the $3^2\Pi$ potential created by the avoided crossing of C' with $B'^2\Pi$, at an internuclear distance where the calculated transition dipole moment between $3\,^2\Pi$ and $X\,^2\Pi$ reaches a sharp maximum, making this the strongest transition to the

ground state from any of the predicted $^2\Pi$ states. The dominant features in the OD spectrum of Fig. 2(c) are thus well explained by the *ab initio* calculations.

It is obvious from Fig. 9 that higher vibrational levels of $C'^2\Pi$—and this includes $v = 0$ of OH—have increasingly large vibrational overlaps with $B'^2\Pi$ and, thus, are rapidly drawn into strong interactions with this state; from the width of the avoided crossing of the two states in Fig. 4 of Ref. 3 one estimates the electronic interaction matrix element at $H \approx 3300\ \text{cm}^{-1}$. In addition, both states can mix with the repulsive $A'^2\Pi$ state from the lower-lying dissociation limit $^1D + {}^2S$. The calculations[10] show that the discrete-continuum interactions lead to efficient predissociation at energies above 11 eV, leaving only the lowest few levels close to the bottom of the C' potential with a real chance for spontaneous emission to the $X^2\Pi$ ground state. The emission, therefore, is likely to be confined to a relatively narrow range of wavelengths, not substantially extending beyond the range covered by the $v' = 0$ progression of OD, and it will be composed of highly irregular band structures that may be difficult to analyze, all the more if the interplay of the three $^2\Pi$ states—one repulsive, the other two stable—leads to 'gaps' in the rotational development of the bands owing to accidental predissociation of individual rovibronic levels. By and large, the characteristics predicted here fit the description of the complex many-line spectra reproduced in Fig. 2 and overlapping the analyzed progression of unperturbed bands.

Transitions from $C^2\Sigma^+$ to high vibrational levels in the ground state[5,6] may possibly be present, but the calculated transition moments are small,[3] and the bands are unlikely to make a significant contribution to the emission near 1850 Å. $C^2\Sigma^+$ ($v = 0$) lies at only $1634.5\ \text{cm}^{-1}$ above $C'^2\Pi$ ($v = 0$). This puts the Σ state into the role of the unique perturber[27] that is largely responsible for the observed Λ-type doubling in the Π state. Pure precession relations[28] predict the spin–rotation interaction γ in $C^2\Sigma^+$ and the Λ-type doubling constant p in $C'^2\Pi$ to be of the order of $0.7\ \text{cm}^{-1}$ and estimate the Λ-doubling constant q at $-0.014\ \text{cm}^{-1}$, comfortably close to the observed values $\gamma = 0.6\ \text{cm}^{-1}$ from Ref. 16 and $p = 0.476\ \text{cm}^{-1}$ and $q = -0.0072\ \text{cm}^{-1}$ from Table III of this work.

A superficial examination of the spectra in Fig. 2 might give the impression that the progression of unperturbed OD bands appearing exclusively in the presence of He represents an isolated transition which shares no common origin with the many-line spectra at overlapping wavelengths. The preceding discussion does not take this view; instead, it associates the progression of red shaded bands with the unperturbed $v' = 0$ level in $C'^2\Pi$ of OD and the large number of unassigned lines, the so-called many-line spectra, with the perturbed levels of OH and OD that escape predissociation. It was pointed out in the first paragraph of this section that the $C'^2\Pi$ levels appear to be populated chiefly in collisions of water molecules with metastable He atoms. What is then surprising is not so much the prominence of a regular progression of unperturbed bands in the spectrum of Fig. 2(c), but rather the persistence in the spectra of Figs. 2(a) and 2(d) of the emission from the perturbed levels of $C'^2\Pi$, in the presence of Ar rather than He and in the absence of any emission from the unperturbed $v' = 0$ state of OD. The explanation may, again, be found in the upper-state interactions with $B'^2\Pi$. This Rydberg state, built on the ground-state configuration of the ion, has a low transition probability to the $X^2\Pi$ ground state,[3,10] but it does provide an alternative route for populating the perturbed rovibronic levels of mixed character that benefit from the larger $C' \rightarrow X$ transition dipole. The excitation may possibly proceed via the formation of OH^+ and OD^+ ions by electron impact on the parent water molecules, followed by recombination with electrons in or near the nozzle throat, in a region of high electron density at only one or two millimeters downstream from the tungsten anode. Interestingly, the spectra of Figs. 2(a) and 2(d) are virtually identical—apart from their higher resolution—with the spectra generated by Smith and Stella[29] using collisions of electrons in a current-modulated beam to dissociatively excite the electronic states of the hydroxyl radical from water molecules.

With the identification of six transitions from the first experimentally established $^2\Pi$ excited state of OD to high vibrational levels in the ground state, we have just barely begun to penetrate the mystery surrounding the long-known many-line emissions of OH and OD near 1850 Å. Indications are that the complexities of these systems arise from Rydberg–non-Rydberg Π–Π interactions of the same kind that have been studied extensively in the spectra of NO (Ref. 30) and N_2 (Ref. 31). Their analyses will be considerably more difficult to achieve, not just because of the familiar problems encountered in spectra characterized by large rotational and vibrational intervals, but primarily because it will be difficult to complement the emission experiments by parallel absorption studies in order to compensate for the lack of emission from the predissociated levels of $C'^2\Pi$ as well as of $B'^2\Pi$. One possibility is laser absorption from vibrationally excited $X^2\Pi$ levels.

ACKNOWLEDGMENTS

It is a pleasure to thank Mr. Frans Alberti and Mr. Chris Harris for their technical assistance during the experimental phase of this work, and Dr. J. K. G. Watson for a critical reading of the manuscript. One of us (F. H.) wishes to acknowledge financial assistance received from the Miescher Fund. Support from the Natural Sciences and Engineering Research Council is gratefully acknowledged for the work performed at Dalhousie University.

[1] (a) K. P. Huber and G. Herzberg, *Constants of Diatomic Molecules* (Van Nostrand Reinhold, New York, 1979); (b) E. de Beer, M. P. Koopmans, C. A. de Lange, Y. Wang, and W. A. Chupka, J. Chem. Phys. **94**, 7634 (1991).
[2] I. Easson and M. H. L. Pryce, Can. J. Phys. **51**, 518 (1973).
[3] E. F. van Dishoeck and A. Dalgarno, J. Chem. Phys. **79**, 873 (1983).
[4] A. Michel, Z. Naturforsch. **12a**, 887 (1957).
[5] P. Felenbok, Annu. Astrophys. **26**, 393 (1963).
[6] P. Felenbok and J. Czarny, Annu. Astrophys. **27**, 244 (1964).
[7] T. Bergeman, P. Erman, and M. Larsson, Chem. Phys. **54**, 55 (1980).
[8] F. Alberti and A. E. Douglas (unpublished).

[9] J. Czarny and P. Felenbok (private communication).
[10] E. F. van Dishoeck, M. C. van Hemert, A. C. Allison, and A. Dalgarno, J. Chem. Phys. **81**, 5709 (1984).
[11] A. D. Sappey and R. A. Copeland, J. Mol. Spectrosc. **143**, 160 (1990).
[12] J. A. Coxon, A. D. Sappey, and R. A. Copeland, J. Mol. Spectrosc. **145**, 41 (1991).
[13] K. P. Huber, C. A. Klug, and F. Alberti, J. Mol. Spectrosc. **124**, 407 (1987).
[14] K. P. Huber and T. Sears, Chem. Phys. Lett. **113**, 129 (1985).
[15] J. M. Brown, J. T. Hougen, K. P. Huber, J. W. C. Johns, I. Kopp, H. Lefebvre-Brion, A. J. Merer, D. A. Ramsay, J. Rostas, and R. N. Zare, J. Mol. Spectrosc. **55**, 500 (1975).
[16] C. Carlone and F. W. Dalby, Can. J. Phys. **47**, 1945 (1969).
[17] J. A. Coxon, Can. J. Phys. **58**, 933 (1980).
[18] J. A. Coxon and S. C. Foster, Can. J. Phys. **60**, 41 (1982); J. Mol. Spectrosc. **91**, 243 (1982).
[19] J. A. Coxon, S. Naxakis, H. Crosswhite, H. M. Crosswhite, A. L. Schmeltekopf, and D. L. Albritton, J. Mol. Spectrosc. **95**, 51 (1982).
[20] J. M. Brown, E. A. Colbourn, J. K. G. Watson, and F. D. Wayne, J. Mol. Spectrosc. **74**, 294 (1979).
[21] C. Amiot, J. P. Maillard, and J. Chauville, J. Mol. Spectrosc. **87**, 196 (1981).
[22] J. A. Coxon (unpublished).
[23] S. R. Langhoff, M. L. Sink, R. H. Pritchard, and C. W. Kern, J. Mol. Spectrosc. **96**, 200 (1982).
[24] S. R. Langhoff and H. Partridge, J. Mol. Spectrosc. **105**, 261 (1984).
[25] J. A. Coxon, J. Mol. Spectrosc. **58**, 1 (1975).
[26] J. K. G. Watson, J. Mol. Spectrosc. **138**, 302 (1989).
[27] R. N. Zare, A. L. Schmeltekopf, W. J. Harrop, and D. L. Albritton, J. Mol. Spectrosc. **46**, 37 (1973).
[28] R. S. Mulliken and A. Christy, Phys. Rev. **38**, 87 (1931).
[29] W. H. Smith and G. Stella, J. Chem. Phys. **63**, 2395 (1975). Notice that the wavelengths given in Fig. 1 of this paper must be revised downward by about 15 Å.
[30] R. Gallusser and K. Dressler, J. Chem. Phys. **76**, 4311 (1982); M. Raoult, J. Chem. Phys. **87**, 4736 (1987); and references given in both papers.
[31] D. Stahel, M. Leoni, and K. Dressler, J. Chem. Phys. **79**, 2541 (1983), and references given in this paper.